

Applicability of Wave Models over Forelands

N. von Lieberman

Franzius-Institut, University of Hannover, Hannover, Germany

S. Mai

Franzius-Institut, University of Hannover, Hannover, Germany

ABSTRACT: Estimation of the wave characteristics in shallow coastal waters, e.g. over forelands in front of sea dikes, can be done – apart from field measurements – using physical and numerical models. The applicability of the numerical models HISWA, SWAN and MIKE21–EMS over forelands was tested in comparison to large scale physical model experiments. All models used (HISWA, SWAN, MIKE21–EMS) gave good approximations of the significant wave height, while the mean wave period was only predicted well using HISWA and SWAN due to program limitations of MIKE21–EMS.

1 INTRODUCTION

In front of the dike – the main protection element at the German North Sea coast – various other protection elements are located. One of these elements is the foreland. Other coastal protection elements in the vicinity of the main dike are, e.g. brushwood fences and summer dikes (Mai et al., 1999).



Figure 1: Changes in wave climate over a foreland (Kramer, 1990)

Forelands reduce the energy of the incoming waves (Fig. 1) and therefore cause a decrease in the wave run-up at the main dike. The amount of a reduction in wave height depends on the foreland geometry, i.e. height, width, and slope of the foreland.

2 EXPERIMENTS IN THE WAVE FLUME

Physical experiments were carried out at prototype scale in the Large Wave Flume “Grosser Wellenkanal” (GWK) of the University of Hannover. The foreland geometry was built of sand. Structures on the foreland, e.g. summer dikes, were covered with concrete to prevent erosion (Fig. 2).

The foreland was located 75 m in front of the wave generator. Its width was 150 m and the height was 1.40 m (Fig. 3). Water-level elevations were measured at 26 positions in the flume in order to calculate the wave characteristics along the foreland. The experiments were carried out with irregular waves with a significant wave height from 0.60 m to 1.20 m and a mean wave period from 2.9 s to 6.7 s using TMA-spectra. The water-levels were varied from 3.0 m to 4.5 m, i.e. 1.6 m to 3.1 m, above the foreland. An example of the wave-characteristics along the foreland is shown in Figure 3 for an incoming wave-field with a height of 1 m and a period of 3.5 s at different water-levels.



Figure 2: Experimental set-up in the GWK

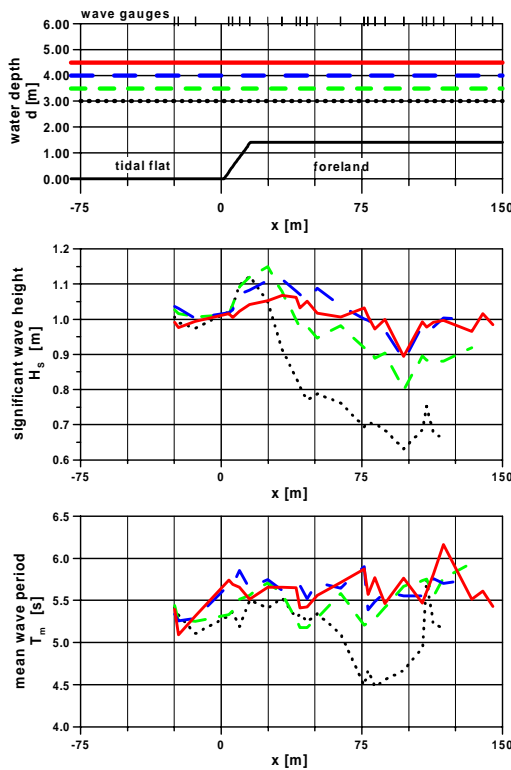


Figure 3: Results of wave propagation (Mai and von Lieberman, 1999)

Directly at the seaward drop of the foreland a large reduction in wave height was revealed. The amount of the reduction caused by wave breaking increased with decreasing water-levels. Especially for a water depth of 1.6 m above the foreland also a reduction of the wave period could be recognized. Both effects are described in the following because of their importance for the design of the sea dike.

3 ANALYTICAL BACKGROUND OF THE NUMERICAL MODELS

The wave model HISWA and the advanced model SWAN are based on the action balance equation. Neglecting the time dependence the action balance equation has the following form (Ris, 1997, Booij et al., 1999):

$$\frac{\partial}{\partial x} c_x N_{(x,y,\sigma,\theta)} + \frac{\partial}{\partial y} c_y N_{(x,y,\sigma,\theta)} + \dots \quad (1)$$

$$\dots + \frac{\partial}{\partial \sigma} c_\sigma N_{(x,y,\sigma,\theta)} + \frac{\partial}{\partial \theta} c_\theta N_{(x,y,\sigma,\theta)} = \frac{S_{(x,y,\sigma,\theta)}}{\sigma}$$

with:

- x, y geographical coordinates
- θ direction of propagation
- σ frequency (in case of missing currents)
- $N_{(x,y,\sigma,\theta)}$ action density spectrum
- $c_x, c_y, c_\sigma, c_\theta$ propagation velocities
- $S_{(x,y,\sigma,\theta)}$ energy source term

The processes of shoaling and refraction are implied in the left hand side of Equation 1 by the definition of propagation velocities $\bar{c} = (c_x, c_y)$.

The processes of dissipation of wave energy due to water-depth induced breaking $S_{ds,br}$ or wave-bottom-interactions $S_{ds,b}$ are included in the energy source term:

$$S_{(x,y,\sigma,\theta)} = S_{ds,br} + S_{ds,b} + \dots \quad (2)$$

Diffraction is not described by the action balance equation and therefore not included in HISWA and SWAN.

The directional wave spectrum is discretized in the frequency and directional domain in SWAN. In HISWA the spectrum is discrete spectral only in the directions and it is parametric in the frequencies introducing the mean wave number k_0 and mean wave frequency σ_0 .

The wave model MIKE21-EMS is based on the elliptic mild slope equation:

$$\nabla(c c_g \nabla \zeta) - \frac{c_g}{c} \frac{\partial^2 \zeta}{\partial t^2} = 0 \quad (3)$$

where the phase velocity is $c = \omega \cdot k$ and the surface elevation is ζ (Madsen and Larsen, 1987). Equation 3 includes the processes of refraction, shoaling and diffraction.

In order to include energy dissipation due to bed friction, wave breaking, and energy loss inside porous structures in MIKE21-EMS, complex harmonic pseudo-fluxes are introduced into Equation 3 (DHI, 1997).

Wave spectra are parameterized in MIKE21-EMS using the rms-value of wave height H_{rms} and the peak period T_p .

The dissipation of wave energy due to bottom friction is determined in all tested models using a quadratic friction law. In HISWA and SWAN the formulation of this bottom friction model is expressed in the following form using the friction coefficient C_{bot} :

$$S_{ds,b(x,y,\theta)}^{HISWA} = -C_{bot} \frac{\sigma_0^2}{g^2 \cdot \sinh^2(k_0 \cdot d)} E_{(x,y,\theta)} \quad (4)$$

$$S_{ds,b(x,y,\sigma,\theta)}^{SWAN} = -C_{bot} \frac{\sigma^2}{g^2 \cdot \sinh^2(k \cdot d)} E_{(x,y,\sigma,\theta)} \quad (5)$$

The bottom friction coefficient is a constant model parameter in HISWA. In SWAN the bottom friction formulation according to Collins (1972) or of Madsen et al. (1988) can be chosen.

In MIKE21-EMS the friction model of Dingemans (1983) is used.

The numerical formulation of wave breaking is described in all models mentioned above according to Battjes and Janssen (1978):

$$D_{br} = \frac{\alpha}{4} Q_b \bar{f} \rho g H_{max}^2 \quad (6)$$

$$\frac{1-Q_b}{\ln Q_b} = -\left(\frac{H_{rms}}{H_{max}}\right)^2 \quad (7)$$

$$H_{max} = \frac{\gamma_1}{k} \tanh\left(\frac{\gamma_2}{\gamma_1} k \cdot d\right) \quad (8)$$

with:

- D_{br} mean dissipation rate per area
- Q_b fraction of breaking waves
- ρ water density
- H_{rms} root mean square of wave height
- H_{max} the maximum wave height
- $\alpha, \gamma_1, \gamma_2$ adjustable coefficients

In HISWA and SWAN the total dissipation rate D is assigned to the dissipation rate for each spectral component (Booij et al., 1985, and Ris, 1997):

$$S_{ds,br(x,y,\theta)}^{HISWA} = -D_{br} \cdot \frac{E_{(x,y,\theta)}}{E_{tot(x,y)}} \quad (9)$$

$$S_{ds,br(x,y,\sigma,\theta)}^{SWAN} = -D_{br} \cdot \frac{E_{(x,y,\sigma,\theta)}}{E_{tot(x,y)}} \quad (10)$$

In MIKE21-EMS the dissipation rate is used to calculate the factor of energy dissipation $e_b \propto D_{br} / E$.

The influence of non-linear processes in wave propagation changing the spectral shape are modeled in HISWA and SWAN, while it is not considered in MIKE21-EMS.

The change in the spectral shape is parameterized by a shift of the mean frequency σ_0 of the parametric wave spectrum in HISWA (Booij et al., 1985). In SWAN triad and quadruplet interactions of the different components of the spectrum are modeled (Ris, 1997).

4 CALIBRATION OF THE MODELS

The models HISWA and SWAN were calibrated using 46 data sets of the flume experiments. For the model MIKE21-EMS 38 data sets were used.

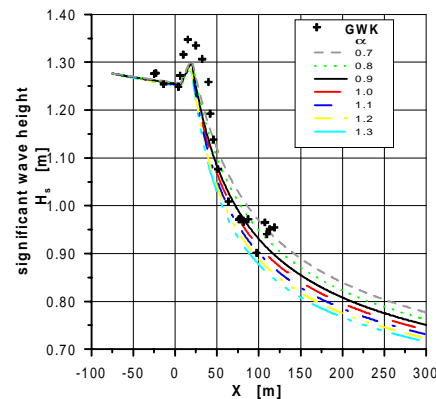


Figure 4: Calibration of the model parameter describing breaking, wave height (model HISWA)

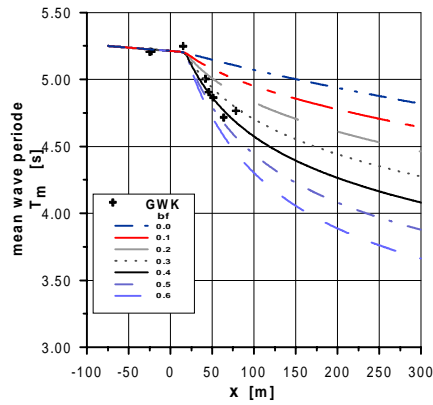


Figure 5: Calibration of the model parameter describing breaking, wave period (model HISWA)

Examples of the calibration of the model parameter α describing breaking (Eq. 6) and the parameter determining the frequency shift are given in the Figures 4 and 5 for a certain set of boundary conditions. The black crosses represent the measurements of the significant wave height (Fig. 4) and the mean wave period (Fig. 5) while the different lines show the results of the numerical model using different model parameters. The solid black line represents the chosen calibration.

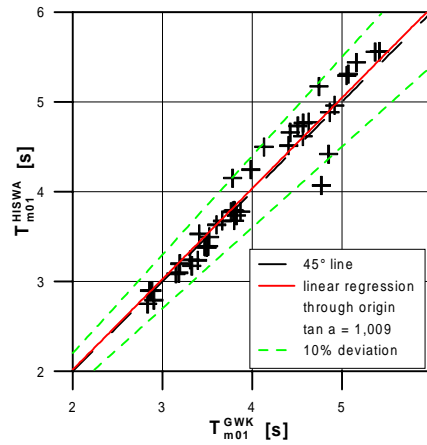
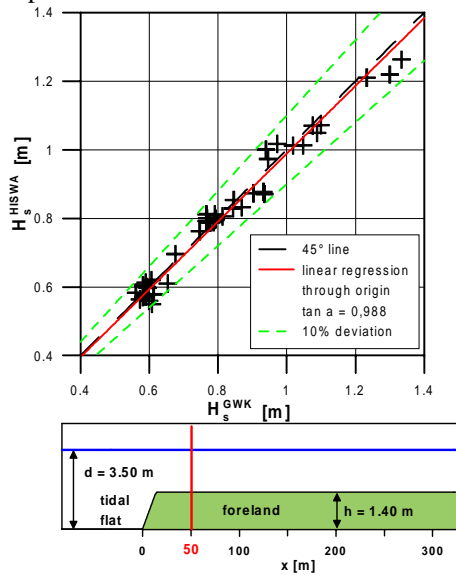


Figure 6: Numerical results compared to physical model tests 50 m behind seaward drop of the foreland for all sets of boundary conditions (46 cases, model HISWA)

Figure 6 shows the correlation of the wave parameter measured in the flume and the results of the model HISWA for all sets of boundary conditions at a position of 50 m behind the seaward drop of the foreland. Both, significant wave height (Fig. 6, top) and mean wave period (Fig. 6, bottom), are represented well by the model. The deviation is less than 10% in all cases tested.

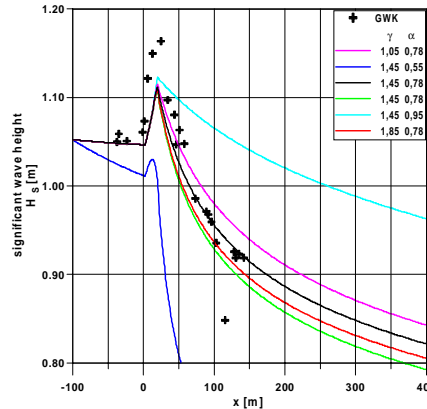


Figure 7: Calibration of the model parameters describing breaking (model SWAN)

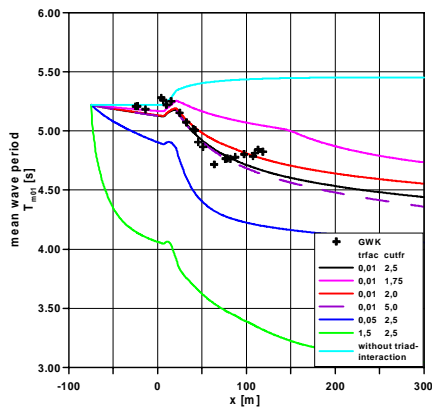


Figure 8: Calibration of the model parameters describing triad-interaction (model SWAN)

The calibration of the model SWAN is shown in the Figures 7 and 8 giving examples for the parameters describing wave breaking α , γ (Eq. 6 to 8) and triad-interaction. The importance of the inclusion of triad-interactions for the description of the decrease in wave period behind the seaward drop is revealed in Figure 8.

In analogy to the results of the model HISWA the quality of the model SWAN is proved correlating the wave parameter significant wave height and mean wave period measured and calculated at certain positions. Figure 9 gives an example of this correlation at a position of 25 m behind the seaward drop.

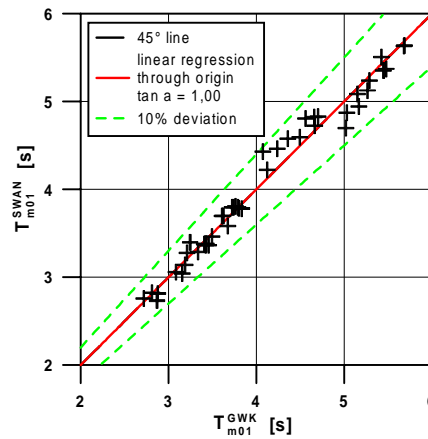
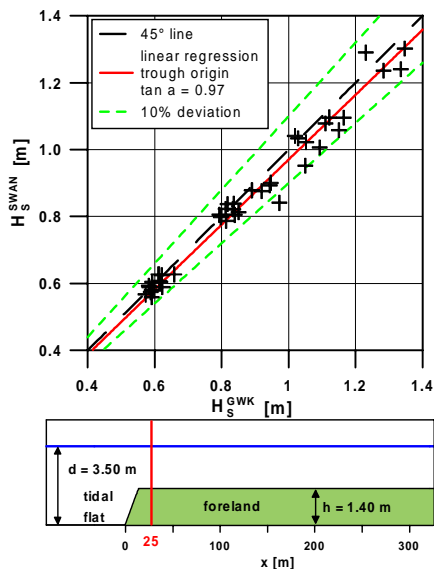


Figure 9: Numerical results compared to physical model tests 25 m behind seaward drop of the foreland for all sets of boundary conditions (46 cases, model SWAN)

In contrast to the models HISWA and SWAN the model MIKE21-EMS cannot reproduce changes in the wave period. As shown in Figure 10 the applicability of the model to describe changes in significant wave height directly at the seaward drop is limited. Measurements and model results differ considerably immediately at the seaward drop of the foreland.

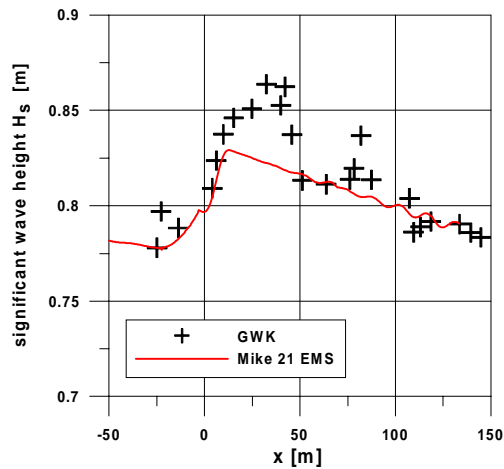


Figure 10: Comparison of significant wave height measured in the flume and calculated with the model MIKE21-EMS

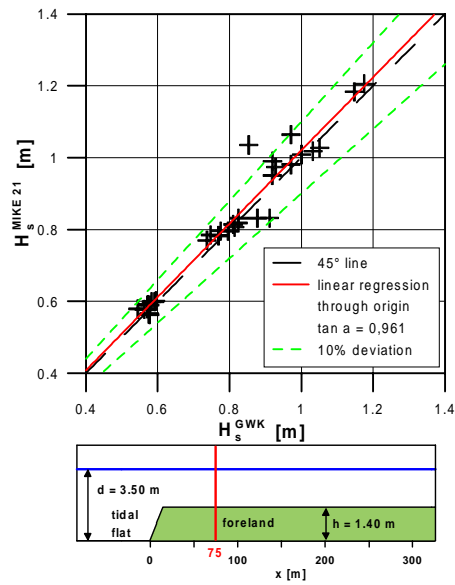


Figure 11: Numerical results compared to physical model tests 75 m behind seaward drop of the foreland for all sets of boundary conditions (38 cases, model MIKE21-EMS)

At a distance of 75 m behind the seaward drop the predictions of the model are again in good agreement with the measurements carried out in the flume. This is also indicated by the comparison shown in Figure 11 based on 38 test sets.

5 RESULTS

Best agreement between measurement and numerical simulation was achieved using the model SWAN. Therefore the following results are based on simulations with this model.

The hydraulic effectiveness of forelands in respect to wave damping can be described with a transmission coefficient, e.g. the relation between transmitted wave height and incoming wave height:

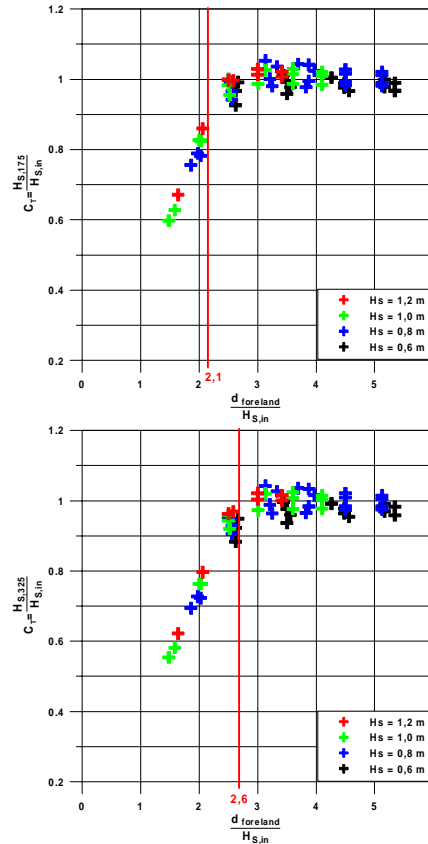
$$c_T = H_{s, x} / H_{s, in} \quad (11)$$

The transmission coefficient of forelands in respect to the wave period can be described analogous to Equation 11:

$$r_T = T_{m, x} / T_{m, in} \quad (12)$$

The influence of the foreland height and the foreland width was investigated introducing the dimensionless parameter $d_{foreland}/H_{s, in}$ with $d_{foreland}$ being the water depth over the foreland and $H_{s, in}$ the incoming significant wave height (Mai and von Lieberman, 1999).

Figure 12 shows the transmission coefficients of a 1.4 m high foreland at a distance of 175 m, 325 m respectively 725 m behind the seaward drop. The transmission coefficient decreases with increasing foreland width, e.g. a transmission coefficient c_T of 90% is related to the dimensionless parameter $d_{foreland}/H_{s, in}$ of 2.1 175 m behind the seaward drop and of 2.6 325 m behind the seaward drop. A foreland width of more than 325 m does not lead to any further reduction of the transmission coefficient.



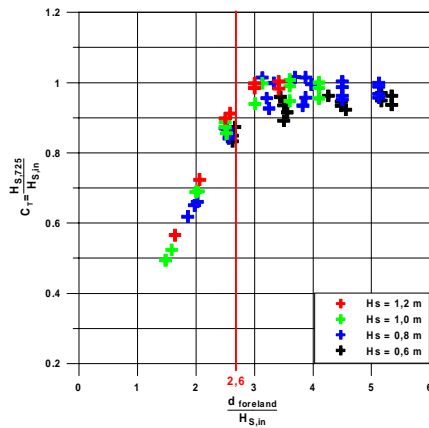


Figure 12: Transmission coefficients of a 1.4 m high foreland 175 m, 325 m respectively 725 m behind the seaward drop – effects of foreland width on wave height (model SWAN)

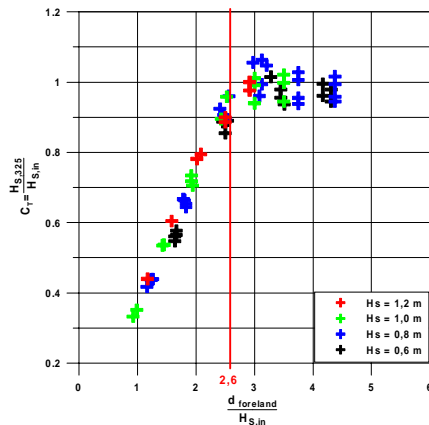
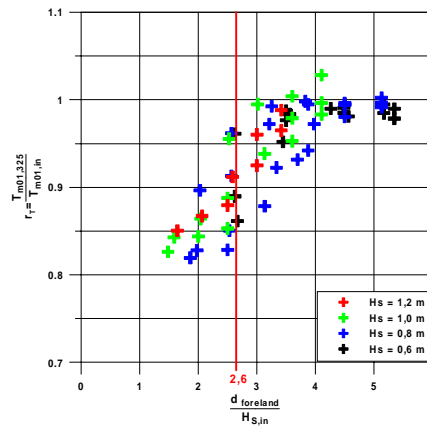


Figure 13: Transmission coefficients of forelands of 1.40 m and 2.00 m height 325 m behind the seaward drop – effects of foreland height on wave height (model SWAN)

The transmission coefficient of a 1.4 m high foreland 325 m respectively 725 m behind the seaward drop in respect to the wave period is given in Figure 14. The transmission coefficient increases almost linearly with increasing ratio $d_{\text{foreland}}/H_{s,\text{in}}$ up to $d_{\text{foreland}}/H_{s,\text{in}} = 3$. In Figure 14 almost no influence of the foreland width can be seen for a width of more than 325 m.

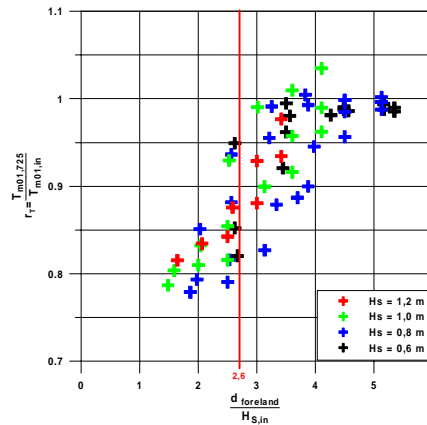


Figure 14: Transmission coefficients of forelands 325 m respectively 725 m behind the seaward drop – effects of foreland width on wave period (model SWAN)

6 CONCLUSIONS

The numerical models HISWA, SWAN and MIKE21-EMS can be used for description of the wave propagation along forelands in respect to the significant wave height. The wave period is only described in the models HISWA and SWAN. After calibration the results of both models are in good agreement with the measurements in the wave flume.

Using the numerical model SWAN in addition to the physical model tests it was found that a width of the foreland of 325 m is sufficient to provide an optimal damping of the waves.

REFERENCES

- Battjes, J.A., Janssen, J.P.F.M.: Energy Loss and Set-up due to Breaking of Random Waves. Proc. 16th ICCE, Hamburg, 1978.
- Booij, N., Holthuijsen, L.H., Herbers, T.H.C.: The Shallow Water Wave Hindcast Model HISWA, Part I: Physical and Numerical Background, Communications on Hydraulic and Geotechnical Engineering. Report No. 85-6, 1985
- Booij, N., Ris, R.C., Holthuijsen, L.H.: A Third-generation Wave Model for Coastal Regions, 1. Model Description and Validation. J. of Geophys. Research, Vol. 104, No. C4, 1999.
- Collins, J.I.: Prediction of Shallow Water Spectra. J. Geophys. Res., Vol. 77, No. 15, p. 2693-2707, 1972
- Danish Hydraulic Institute (DHI): MIKE21: Elliptic Mild-Slope Wave Module. Release 2.6. Horsholm, Danmark, 1997
- Dingemans, M.W: Verification of Numerical Wave Propagation Models with Field Measurements, CREDIZ Verification Haringvliet, Rep. W488, Part 1b, Delft Hydraulics, Delft, 1983
- Kramer, J.: Sturmfluten, Küstenschutz zwischen Ems und Weser. 6. überarb. Aufl., Verlag Soltau GmbH, Norden, 1990.
- Madsen, P.A. and Larsen, J.: An Efficient Finite-Difference Approach to the Mild-Slope Equation. Coastal Engineering, Vol. 11, p. 329-325, 1987.
- Madsen, P.A. et al.: Spectral Wave Attenuation by Bottom Friction: Theory. Proc. 21st Int. Conf. Coastal Eng., ASCE, p. 492-504, 1988
- Mai, S., von Lieberman, N., Zimmermann, C.: Interaction of Foreland Structures with Waves. XXVIII IAHR Congress, Graz, 1999.
- Mai, S., von Lieberman, N.: Effectiveness of Forelands Reducing the Wave Load on Dikes. 2nd Chinese Joint Seminar on Recent Developments in Coastal Engineering, Tainan, p. 293-305, 1999.
- Ris, R.C.: Spectral Modeling of Wind Waves in Coastal Areas, Communications on Hydraulic and Geotechnical Engineering, Report No. 97-4, 1997.